Influence of particle surface roughness on creeping granular motion

Li-Tsung Sheng, Wei-Ching Chang, and Shu-San Hsiau*

Department of Mechanical Engineering, National Central University, 300 Jhongda Road, Jhongli 32001, Taiwan

(Received 5 February 2016; revised manuscript received 8 May 2016; published 11 July 2016)

A core is formed at the center of a quasi-two-dimensional rotating drum filled more than half with granular material. The core rotates slightly faster than the drum (precession) and decreases in radius over time (erosion) due to the granular creeping motion that occurs below the freely flowing layer. This paper focuses on the effect of the surface roughness of particles on core dynamics, core precession, and core erosion. Two different surface roughness of glass particles having the same diameter were used in the experiments. The surface structures of the particles were quantitatively compared by measuring the coefficients of friction and using a simple image contrast method. The experiments were performed with five different filling levels in a 50-cm-diameter rotating drum. According to the results, core precession and core erosion are both dependent on the particle surface roughness. Core precession becomes weaker and erosion becomes stronger when using particles having a rough surface in the experiments. To explain the physics of core dynamics, the particles' surface roughness effect on the freely flowing layer and the creeping motion region were also investigated. The granular bed velocity field, maximum flowing layer depth δ, shear rate in the flowing layer $\dot{\gamma}$, and the creeping region decay constant y_0 were also calculated in this paper. The effect of the particles' surface roughness on these physical variables well illustrates the physics of core dynamics and creeping granular motion.

DOI: 10.1103/PhysRevE.94.012903

I. INTRODUCTION

Granular materials can pile at rest with a slope lower than the angle of repose. The dry particle layers are stably stacked by the force of asperities interlocking between the particles. When the slope of the pile is larger than the angle of repose, the behavior of the particles changes from a solidlike phase to a fluidlike phase. This means that the particles are no longer at rest, especially those near the upper surface of the pile. Moreover, a flowing surface layer is formed when particles collapse on such a granular pile; a stationary bulk region can also be found below this flowing surface layer. This stationary bulk region is traditionally called a "fixed bed" region. Many studies have been conducted under such an assumption [1–4]. However, defining the boundary between the flowing layer and fixed bed region is difficult. This is because there are some particles with very slow velocities between these two regions, and such slow motion can be detected with an arbitrary depth. This creeping motion region below the flowing layer has been measured by Komatsu *et al.* [5]. They also found that the velocity linearly decreased with depth in the flowing layer and exponentially decreased with depth in the creeping motion region.

To measure the dynamics of the creeping granular flow, a long time-scale measurement to detect the slow velocities is necessary. For this purpose, a circular rotating drum can provide a constant driving force (with a constant rotating speed), producing a continuous granular avalanche over a long time. When the drum rotates, particles are continuously carried to the upper part of the inclined free surface, collapsed down the slope, and deposited again in the fixed bed. A lenslike flowing layer is formed near the inclined free surface. The maximum depth δ of the flowing layer is at the center of the flowing layer, which is typically 3–12 particle diameters deep [3,6–9]. δ can be influenced by several physical variables, such as particle characteristics, the rotation speed, and size of the drum. However, it is well known that particle segregation and mixing behavior occur in the flowing layer when particles with different properties are filled into the rotating drum. Therefore, when the rotating drum is filled with identical particles with different colors, granular mixing will occur in the flowing layer via the collapse of such particles through the flowing layer. In such cases, when the rotating drum is filled with half or less of such particles, the particles will completely mix after a few revolutions, because all particles will have passed through the flowing layer several times. However a completely different situation occurs when the drum is more than half filled; an unmixed circular region can be found at the center of the drum. This is because in this situation, even after many revolutions, the particles in the unmixed circular region never pass through the flowing layer.

The "core" (unmixed circular region) is formed after the first four or five revolutions of the drum and is close to (beneath) the flowing layer. Hence, investigating creeping granular motion by studying the dynamics of the core is convenient [9–11]. The core should exhibit a solidlike rotation with the drum since it never passes through the flowing layer. However, there are many studies that show the core is dynamic [9–12]. It has been found that after many revolutions, the core rotates slightly faster than the drum (precession) and decreases in radius over time (erosion) due to granular creeping motion. McCarthy *et al.* [10] reported that the core precession is linear and depends on the particle characteristics and shape of the container. Socie *et al.* [9] experimentally investigated the core precession and erosion. They developed a model, which is based on an exponential velocity profile below the flowing layer and the shear rate in the flowing layer, to predict the dynamics of the core. Socie *et al.* also found that core precession linearly depends on the number of drum revolutions, while core erosion logarithmically changes with the number of drum revolutions. Arndt *et al.* [11] investigated

*Corresponding author: sshsiau@cc.ncu.edu.tw

the core dynamics under different gravitational levels. They reported that core precession is dependent on the shear rate of the flowing layer and that the erosion is independent of the shear rate of the flowing layer. Arndt *et al.* [11] also argued that erosion is a local diffusional effect in the creeping motion region and is not affected by the flowing layer.

While the particles' properties have a critical effect on the granular flow, the influence of particles' surface characteristics has rarely been discussed in most granular flow studies, especially in investigations on such creeping granular motion. This is because the surface properties of particles, e.g., surface roughness, has usually been assumed to have minor effects and is less important than some significant properties of particles, i.e., the particle shape, size, and density. Only a few experimental studies have investigated the effect of particle surface roughness on granular flow. Pohlman *et al.* [13] investigated the effect of nanoscale variations on the surface roughness of particles on granular flow in a rotating drum. They found that the dynamic angle of repose is greater for rough particles than that for smooth particles. They also indicated that the influence of the particles' surface roughness is difficult to quantify solely in terms of the coefficient of friction. Plantard *et al.* [14] reported an investigation on surface-roughness-induced granular segregation in a slurry system under shear driving force. They found that rough particles behave similar to smooth but larger particles in the mixture system with smooth and rough particles. Liao *et al.* [15] demonstrated an experimental study to investigate the influence of intruder surface roughness on the Brazil nut effect in a vibrating granular bed. They found that the Brazil nut effect is alleviated by the rougher intruder surface due to greater kinetic energy dissipation.

However, there are still some macroscopic properties that can reflect the effect of surface roughness on granular flow, e.g., the angle of repose, coefficient of friction, and restitution coefficient [13,15–17]. More importantly, in the subsurface creeping motion region, the influence of surface roughness of particles should be more obvious, because the particles are denser in this region and the asperities interlocking between particles may be greater. To investigate the influence of surface roughness of particles on the dynamics of creeping granular motion, conclusions should also be based on long-time-scale experiments. In this paper, we will explore the dependence of creeping flow on different surface roughness of particles by measuring the core precession and erosion in a rotating drum. The dependence of the core dynamics on the particle filling levels will also be discussed. A model developed by Socie *et al.* [9] will be adopted to investigate the physics of core dynamics in this paper.

II. EXPERIMENTAL PROCEDURE

A. Surface structures of the particles

Spherical particles with a nominal diameter, d, of 4 ± 0.1 mm with two different grades of surface roughness were used in the experiments. The material of particles was glass with a density of 2480 kg/m^3. The smooth particles were produced by an industrial glass-bead manufacturer (Chyuan-Sin Co., Taiwan). The rough particles were produced via a milling process using ball mill equipment with silicon carbide grit. The hardness of glass is 5.5 (Mohs scale of mineral hardness). The hardness of silicon carbide is 9–9.5. When the smooth surface of glass particles and silicon carbide grit mix in the ball mill, some micropores are produced on the surface of glass particles due to the collision of glass and silicon carbide materials. The milling process time was fixed at 10 h to ensure that all glass particles had the same rough surface structures with roughness. In addition, during the ten hours, the shape and size of particles did not experience alterations. A test sieve shaker with proper mesh sizes was also used to confirm that the rough particles had the same diameter as smooth particles. It should be noted here that we limited our particle size to 4 mm. This is because the use of $d < 4$ mm particles to produce surface roughness using a milling process may change the shape and size of particles, and electrostatic forces may interfere with the following rotating drum experiments.

While the particle surface roughness not only influences the surface friction [13], the Coulomb friction coefficient is still a critical property when examining the surface condition of particles in several studies [13,15,18,19]. A commercial Jenike shearing tester was used with ten repeated measurements to measure the friction coefficient between particles. The friction coefficient is 0.56 ± 0.01 for the smooth particles and 0.75 ± 0.02 for the rough particles. The small deviations in the friction coefficient demonstrate that the particles within each group have nearly the same surface roughness.

To further compare the surface roughness of the particles, a simple image contrast method was also used. In this method, a high resolution scanning transmission electron microscope (JEM-2100, JEOL) was used to capture magnified images of a particle's surface. The surface profiles of particles were then described by calculating the pixel-value contrast of the magnified images. Figure 1 shows 1500× magnified images of smooth and rough particle surfaces, and Fig. 2 shows the pixel-value contrast for each pixel grid (i, j) in the magnified images (size of $M \times N$ pixels, where $M = 640$ and $N = 480$). Figure 2 shows that the pixel-value contrast distribution of the rough particles was sharper than that of the smooth particles. Here, we define the "root mean square pixel-value contrast" P_q, which is similar to the well-known RMS roughness, to quantify the surface roughness of particles. It can be shown as

$$P_q = \frac{1}{M \times N} \sum_{i=1}^{M} \sum_{j=1}^{N} \sqrt{\{[P_{cij}(i,j)] - (P_{\text{cave}})\}^2}, \qquad (1)$$

where P_{cij} is the pixel-value contrast for each pixel grid (i, j) in the magnified image. P_{cave} is the average value of the pixel-value contrast of all the pixel grids in the magnified image. P_{cij} and P_{cave} can be represented as

$$\begin{aligned} P_{cij}(i,j) &= P_{ij}(i,j) - P_{\min}, \\ P_{\text{cave}} &= \frac{1}{M \times N} \sum_{i=1}^{M} \sum_{j=1}^{N} P_{cij}(i,j), \end{aligned} \qquad (2)$$

where P_{ij} is the pixel value for each pixel grid (i, j) of magnified image and $P_{\min}$ is the minimum value of the pixel value of all the pixel grids in the magnified image.

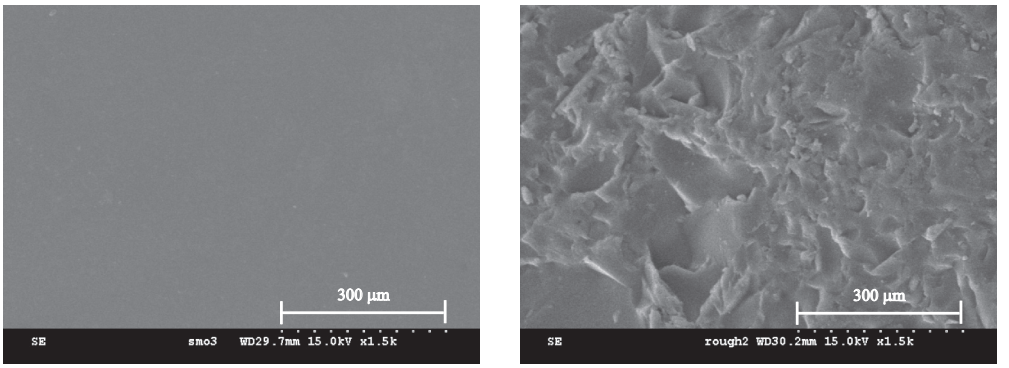

(a) (b)

FIG. 1. Images of the surface profile of particles observed using a high resolution scanning transmission electron microscope: (a) 1500× magnification for a smooth particle; (b) 1500× magnification for a rough particle.

In this study, P_q was 13.8 ± 0.13 for the smooth particles and 52.9 ± 0.38 for the rough particles. The standard deviations in P_q were obtained via ten different calculations from ten 1500× magnified images that were captured from ten individual smooth (or rough) particles. The small deviations of P_q (0.7% for rough particles and 0.9% for smooth particles) also show that the particles within each group have nearly the same surface roughness. However, the value of P_q for the rough particles was much larger than that of the smooth particles. This means that the surface structures of the rough and smooth particles were quite different.

It should be noted here that even though the rough particles have nearly the same surface roughness after the milling process, they can only be used for a limited time because the surface structure changes with experimental use. Therefore, we always measured the coefficient of friction of particles after every experimental test using a shearing tester. If the surface properties were altered, new rough particles were produced with similar surface roughness as the older particles for use in the next experimental test.

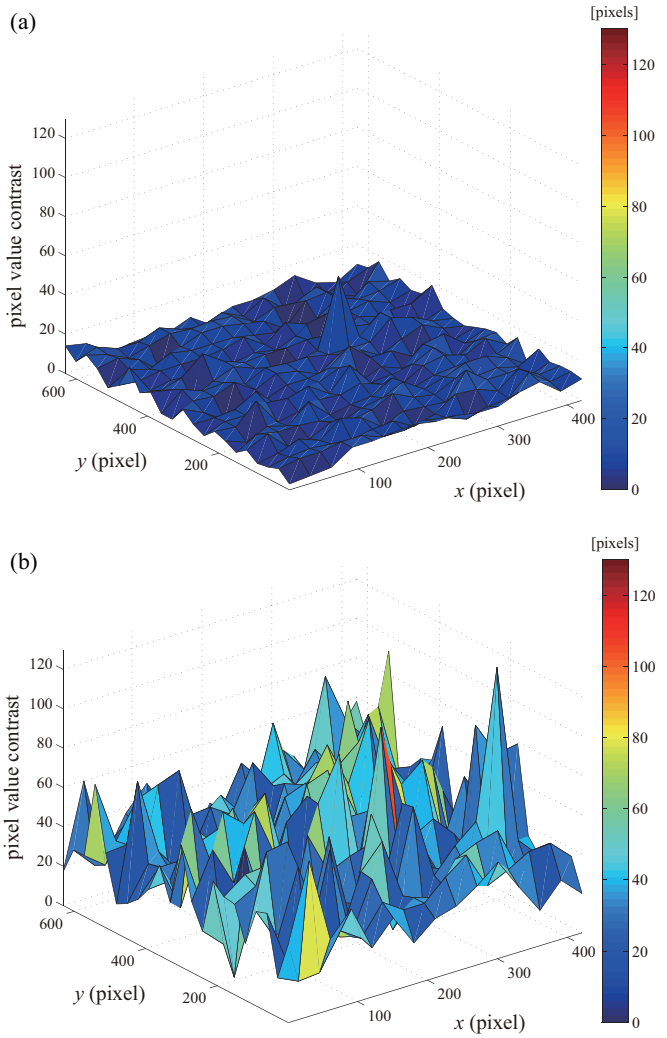

FIG. 2. The pixel-value contrast distributions from 1500× magnified images of particle surfaces: (a) smooth particle; (b) rough particle.

B. Digital photography equipment

To measure the long time-scale dynamics of the core, images of the arrangement structure of bicolor particles in the rotating drum were recorded. A high memory capacity (240 GB) digital HD video camera (SONY, HDR-XR550, polychrome, with a shooting frame rate of 30 fps and a resolution of 1920 × 1080 pixels) was mounted concentric with the axis of the drum to record the evolution of the core erosion and precession over 10 h. Furthermore, for the purpose of investigating the mechanism of core erosion and precession, the velocity fields of particles were measured using particle-image velocimetry (PIV). The details of the procedure used for PIV analysis in this paper are provided in the Appendix. A high-speed CMOS camera (IDT MotionPro Y3 plus, monochrome, with a shooting frame rate of 2000 fps and a resolution of 1280 × 1024 pixels) was used to record the sequential motion of the particles to support the PIV calculation. The shear rates in the flowing layer and creeping motion region were also obtained from the velocity fields. Four high-luminance LED lamps (100 W, 6000 K) were used to illuminate the particles in the rotating drum.

C. Circular rotating drum

Experiments were performed in a quasi-two-dimensional rotating drum. Jain *et al.* [20] argued that for a quasi-two-dimensional rotating drum, the thickness of the drum should be larger than $3.2d$ to eliminate the front and back wall friction but should also be thin enough ($\leqslant 9.4d$) [9,11] to suppress the axial directional motion of particles. The rotating drum in this paper, which had an inner diameter of 50 cm and a thickness of 1.5 cm ($\approx 3.75d$), was made of Plexiglas with transparent glass front and back faceplates to enable the collection of experimental images. The inner circumferential Plexiglas wall of the drum was covered with 40-grit sandpaper to prevent the particles sliding with respect to the circumferential wall of the drum. The drum is shown in Fig. 3 with the coordinate system and its related parameters, which will be introduced in more detail in the next section (Sec. III).

Five filling levels were used to investigate the creeping granular motion. With the rotating drum being defined as a quasi-two-dimensional system, the filling level is defined as the ratio of the area occupied by the granular material to the total drum area [21–23]. They were $f = 0.623$, 0.662, 0.707, 0.746, and 0.778, where f is the filling level. At the beginning of experiments, the drum was filled with only smooth (or only rough) glass particles to the desired filling level. The left half had black particles, and the right half had white particles. In such a situation, the interface between black and white particles is a vertical line from the front view of the drum (see the initial condition image in Fig. 4). The rotating frequency was set at one revolution per minute (rpm). The flow regime in the drum was the rolling regime [24–28] under the rotation frequency and size of the drum in this study. In the rolling regime, the flow is continuous and free surface of the flowing layer remains flat.

The core is defined as the circular domain of unmixed particles at the center of the rotating drum. The core circle is typically not a perfect circle on the experimental image, especially for cases with a smaller filling level. Here, to obtain a meaningful core circle, ten repeated calculations were performed using the method of three points defining a circle and its diameter. The three points are chosen randomly at the boundary between the mixing and unmixed regions, i.e., the boundary of the core. The boundary is defined using image analysis based on binarized images. Therefore in ten repeated calculations, 30 different points are chosen randomly at the boundary of the core. The standard deviation of the resulting average diameter of the core circle is about $\pm 4\%$. Hence, the core radius was measured from the average value of the ten circles' radii. The core erosion was measured using the variation in the average radius with passing time.

After the first five revolutions, the core forms and interface between white and black particles will rotate at certain angles

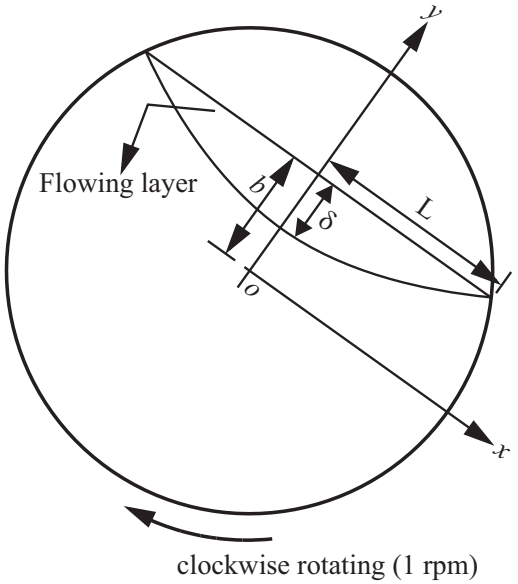

FIG. 3. A schematic of the rotating drum with the coordinate system and its related parameters.

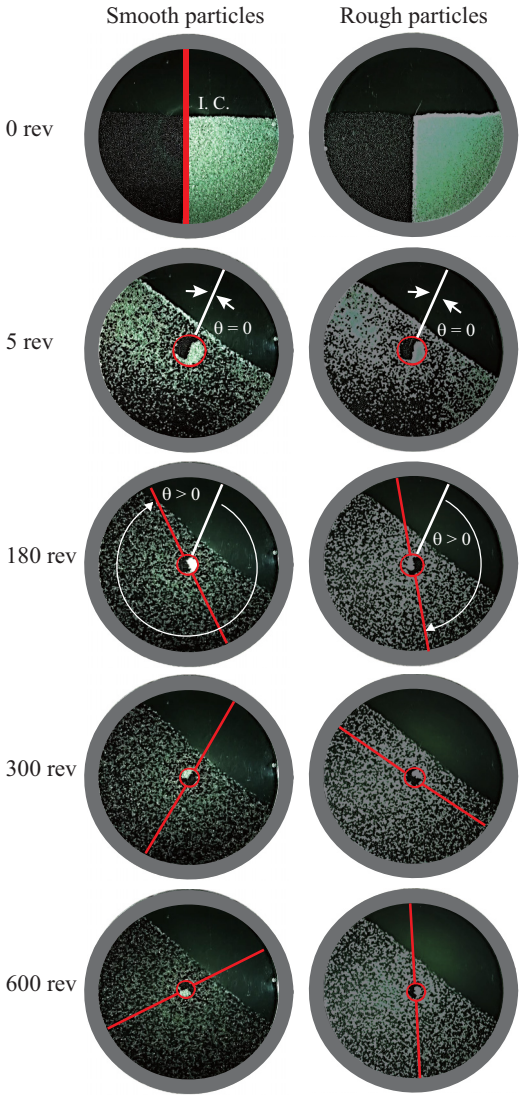

FIG. 4. Experimental images of the evolution of the core after 0, 5, 180, 300, and 600 complete revolutions with a filling level of $f = 0.662$ for the smooth (left-hand column) and rough (right-hand column) particles. The drum rotated clockwise at a frequency of 1 rpm. The figure also shows the representations of the precession angle θ.

(around 20°–25°) from the initial vertical line (see Fig. 4). Here, we define the precession angle θ as the angle between the interface after N revolutions and after the first five revolutions, i.e., $\theta = 0$ after first five revolutions of the drum (see the representation of the precession angle in Fig. 4). Since the interface is curved near the edge of the core, only the central 60% of the interface was used to determine the precession angle. Compared with previous studies by Socie *et al.* [9] and Arndt *et al.* [11] regarding core precession, there was a smaller portion of the interface in this study that can be used (Socie *et al.* [9] had 75% and Arndt *et al.* [11] had 70%). This is because in this study, the particle size relative to the core size was larger than in previous studies. If each particle close to the front faceplate of the drum is regarded as a pixel point in an experimental image of the bicolor particles' arrangement structure, a larger ratio between the particle size and core size may cause a lower resolution of the core in such an experimental image. The resolution may be associated with the accuracy of line-fitting analysis for the interface. Therefore, due to the lower resolution of the core, only the central 60% of the interface in this study could be used to fit the line of the interface and to determine the precession angle.

III. RESULTS

Figure 4 shows the typical evolution of the core after 0, 5, 180, 300, and 600 complete revolutions with a filling level of $f = 0.662$ for the smooth and rough particles. The drum rotated clockwise at a frequency of one rpm. During the initial condition, the interface between black and white particles can be clearly defined as a vertical line. The core formed after the first five revolutions of the drum. The precession angle is defined as equal to zero after the first five revolutions of the drum. The straight red lines in Fig. 4 for a different number revolutions represents the angular position of the interface in the core, and the red circles indicate the size of the core. From Fig. 4, after 180 complete revolutions of the drum, it can be seen that θ increases (core precession) and the core size becomes smaller (core erosion). After 300 complete revolutions, the precession angle for the smooth particles was even larger than 360°. This means that the number of revolutions of the core is one revolution more than the drum after 300 complete revolutions of the drum. However, it also can be seen clearly that the core precession alleviated for the rough particles.

Figure 5 illustrates the dependence of the precession angle θ on the number of revolutions of the drum N for the smooth and rough particles for five filling levels. All experiments were performed for the first 600 revolutions of the drum, excluding the case of the smallest filling level, $f = 0.623$, which was performed only for the first 360 revolutions of the drum. This is because the core in this case ($f = 0.623$) was too small after the first 360 revolutions, resulting in difficulty in defining the interface between the two different colors of particles. As shown in Fig. 5, the precession angles linearly increased with the number of revolutions. The rate of increase of the precession angle for small filling levels was greater than for large filling levels. More importantly, a rough surface resulted in a smaller precession angle, regardless of the filling levels.

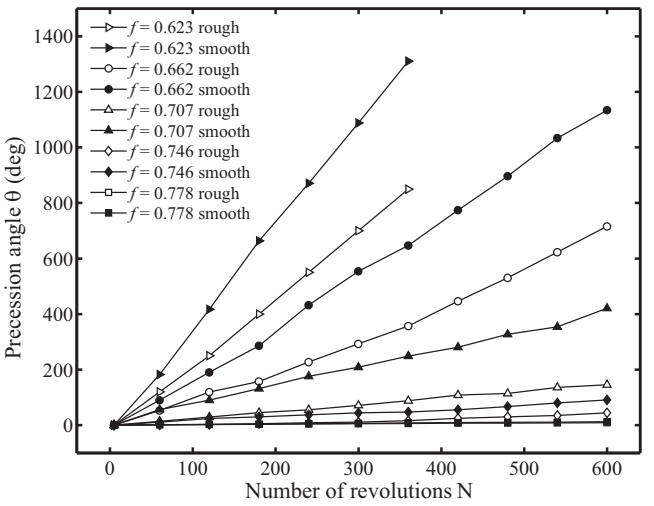

FIG. 5. The dependence of the precession angle θ on the number of revolutions of the drum N for the smooth and rough particles for five filling levels. All experiments were performed for the first 600 revolutions of the drum, excluding the case of the smallest filling level, $f = 0.623$, which was only performed for the first 360 revolutions of the drum.

The discrepancy in the precession angle due to particle surface roughness is more obvious when the filling level was small.

The dimensionless precession rate m is defined as the change in the precession angle (in radians) per radian of drum revolution. In other words, m is the slope of the data in Fig. 5. Figure 6 shows the values of m for smooth and rough particles for five filling levels. As shown in Fig. 6, the precession rate was larger for a small filling level and went to zero for a high filling level. The dependence of the precession rate on the filling level in Fig. 6 is consistent with the results of Socie *et al.* [9]. More importantly, the precession rate was highly sensitive to the surface roughness at a small filling level while

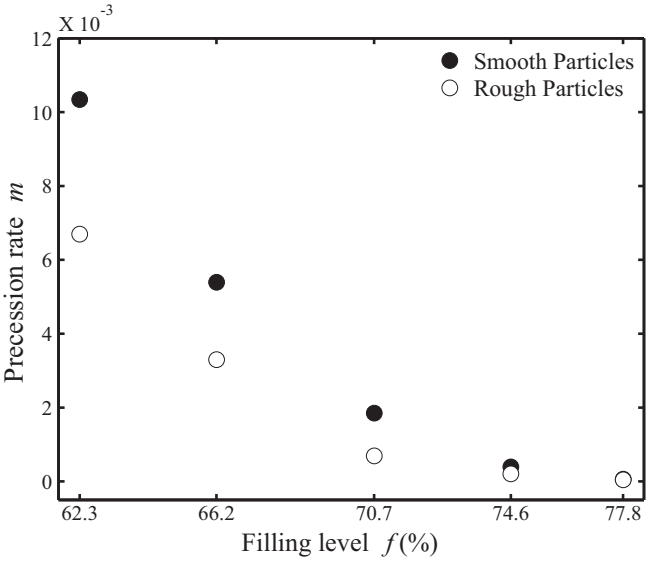

FIG. 6. Dimensionless precession rate m for smooth and rough particles as a function of the filling levels f.

the surface roughness effect on the precession rate can be ignored for the highest filling level.

To investigate the physics of the results in Fig. 6, a model of core dynamics, which was derived by Socie *et al.* [9], was adopted to investigate the core precession and erosion. This model is based on a two-region velocity field, wherein the particle velocity is assumed to linearly decrease with depth in the flowing layer [5,29] and to exponentially decrease with depth in the creeping motion region below the flowing layer [5,6,9,30]. According to such an assumption of velocity profile, the precession rate m can be represented as [9]

$$m = \frac{\dot{\gamma}}{4\pi\nu} e^{(\delta - b)/y_0}, \tag{3}$$

where $\dot{\gamma}$ is the shear rate in the flowing layer, b is the distance from the center of the drum to the center of free surface of the flowing layer (see Fig. 3), ν is the rotation frequency, which was set at 1 rpm in this study, and y_0 is a decay constant for the creeping flow velocity profile. Since ν is constant (1 rpm) and b does not depend on the particle surface roughness, m is a function of certain variables in Eq. (3), i.e., $\dot{\gamma}$, δ, and y_0. Hence, the dependence of surface roughness influence on these variables will be closely examined in the following discussion to obtain a clear understanding of the effect of the particle surface structure on m.

The primary features of the core dynamic model [9] is the two-region velocity field. To analyze the physical variables $\dot{\gamma}$, δ, and y_0, the velocity field in the flowing layer region and creeping motion region must first be measured. Figure 7 shows the time-averaged velocity field of the granular bed for smooth particles with a filling level of $f = 0.662$ obtained using PIV measurements. A lenslike flowing layer could be found at the top of the granular bed. For further analysis, the velocity profile distribution along the path from the center of the drum to the center of the free surface of the flowing layer was obtained from the data of the results in Fig. 7. Figure 8 shows the two-region particle velocity profile for smooth and rough particles having $f = 0.662$. The error bars on the velocity profile are calculated from the deviation of the granular velocity with time. The particle velocity linearly decreased with depth in the flowing layer region and exponentially decreased with depth in the creeping motion region. Figure 8 shows that the deviations in the velocity are small in the creeping region and large

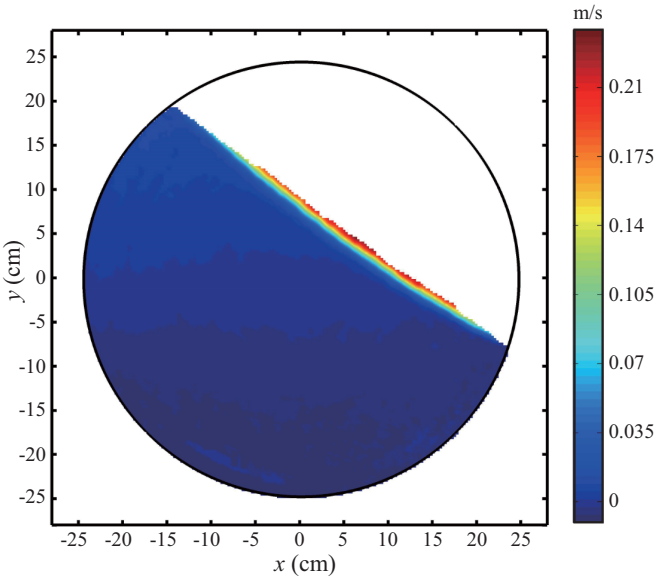

FIG. 7. The time-averaged velocity field of the granular bed in the drum for smooth particles having $f = 0.662$ obtained using PIV. A lens-like flowing layer region can be seen at the top of the granular bed.

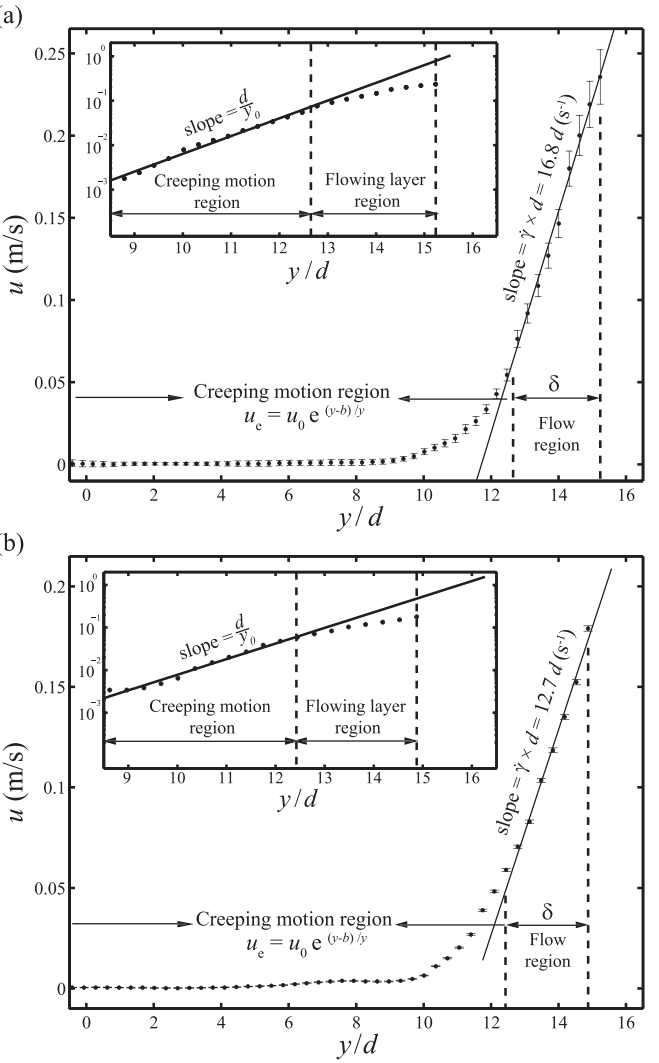

FIG. 8. Two-region particle velocity profile with $f = 0.662$: (a) for the smooth particles and (b) for the rough particles. The particle velocity linearly decreased with depth in the flowing layer region and exponentially decreased with depth in the creeping motion region. The inset shows the exponential velocity profile in the creeping motion regime with a logarithmic ordinate (logarithmic velocity value). The velocity profile in the creeping region u_e can be described using $u_e = u_0 e^{(y-b)/y_0}$ with $u_0 = 78.64$ cm/s, $y_0 = 1.09d$, and $b = 15.23d$ for the smooth particles, and $u_0 = 47.88$ cm/s, $y_0 = 1.18d$, and $b = 14.97d$ for the rough particles. The error bars are calculated from the deviation in the granular velocity along with time. The deviation in the velocity for the rough particles is smaller than that for the smooth particles because of the larger kinetic energy dissipation.

in the flowing layer region. This is because the particles in the flowing layer have large granular temperature and large velocity fluctuation intensity. Comparing the effect of surface roughness, it can be inferred that the deviations in the velocity for the rough particles are smaller than the deviations of the velocity for the smooth particles, due to larger kinetic energy dissipation and smaller granular temperature in the rough particle.

It should be noted here that the basic definitions of the flowing and creeping regions are that the velocity profile is a linear distribution in the flowing layer region and is exponentially decaying in the creeping region. However, more importantly, we have to define the exact location of boundary between these two regions for further analysis. It is easy to approximately discriminate between these two regions from the velocity profile shown in Fig. 8. However, several repeated linear fittings for the velocity profile in the flowing layer are made by choosing different positions near the interface as the boundary for these repeated fittings. By comparing the standard deviation of these fittings, we can define the exact location of the boundary between the two regions.

We calculated the value of b from the experimentally acquired images using image analysis. The free surface of the flowing layer is not always a flat surface. Under this situation, fluctuations exist in the value of b with time. The final mean values of b are obtained by averaging all values of b acquired during the experimental process. Therefore, there is a trivial difference between the average values of b for different experimental cases with the same f because of the fluctuations in the values of b . For example, the difference in b value in the case of $f = 0.662$ for the smooth and rough particles, as mention in the caption of Fig. 8, is only 0.26 times the particle diameter.

The shear rate $\dot{\gamma}$ can be obtained by calculating the velocity decrease rate with depth in the flowing layer, i.e., the slope of the velocity profile distribution in the flowing layer region [see Fig. 8(a)]. The velocity profile in the creeping region u_e can be described using $u_e = u_0 e^{(y-b)/y_0}$ [5,9,30,31] due to its exponential decay with depth, where y is the distance between the center of the drum and the discussing position, and its direction is from the center of drum to the center of the free surface of the flowing layer. u_0 is a velocity constant. The inset of Fig. 8(a) shows the exponential velocity profile in the creeping motion regime with a logarithmic ordinate (logarithmic velocity value). Based on the representation of u_e, the slope of the exponential velocity profile in the inset of Fig. 8(a) can be shown as d/y_0. The velocity profile obtained via the same analysis method for rough particles with $f = 0.662$ is shown in Fig. 8(b), and other cases with different filling levels for smooth and rough particles were also calculated to obtain $\dot{\gamma}$, y_0, and δ.

The maximum flowing layer depth can be calculated using $\delta = y_0 \ln(u_0/\dot{\gamma} y_0)$ [9], where u_0, $\dot{\gamma}$, and y_0 can be calculated from the velocity profile as shown in Fig. 8. This representation of δ is derived from the definition of the slope of the velocity profile at the boundary between the two regimes (flowing layer region and creeping motion region), wherein which the slope of the velocity profile has to be consistent with both the slope in the flowing layer region and in the creeping motion region. However, it should be noted that because the initial core

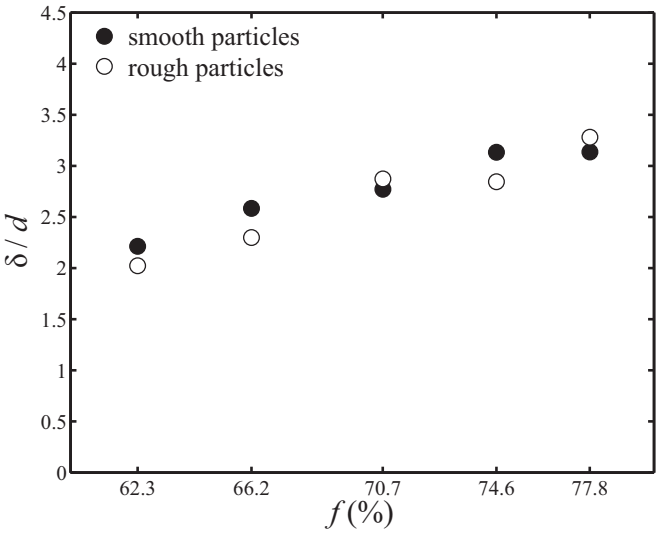

FIG. 9. The maximum flowing layer depth δ for smooth and rough particles as a function of the filling levels f.

forms close to (beneath) the flowing layer, Arndt *et al.* [11] calculated the maximum flowing layer depth using $\delta = b - r_0$, where r_0 is the initial radius of the core. In this study, we also calculated δ using this method; the results of the two different methods have an acceptable minor difference, which is small than 10%. However, for being consistent with the definition of δ in the two-region velocity field model, the results of δ that were calculated from velocity profiles will be adopted for the following discussion in this study.

Figure 9 shows the maximum flowing layer depth for the smooth and rough particles for five filling levels. It can be seen that the flowing layer depth slightly increased with the filling level. The reason is that when the filling level is large, the particles near the center of the free surface have a greater rotational inertia due to the rotating driving force of the drum with a longer radius of gyration under the same rotating frequency (1 rpm). Here the rotational inertia of particles is caused by the revolution of particles around the center of the drum. Particles with greater rotational inertia can possess greater rotational kinetic energy. When the particles slide down along the free surface, the greater rotational kinetic energy of the particle revolution motion can transfer to greater linear kinetic energy. Hence, more particles can overcome the maximum static friction due to the greater linear kinetic energy and start to flow with a larger f. For this reason, this may result in a thicker flowing layer depth with a large f. However, more important to this discussion is that the maximum flowing layer depth is essentially independent of the particle surface roughness. Two contrary effects compete with each other to cause the similar δ for the smooth and rough particles when the filling levels were the same. One effect is that the rough particles cause a larger dynamic repose angle of the granular bed in the rotating drum via stronger asperities interlocking between particles. When the rough particles slide down along the larger inclined slope angle of the granular bed, the particles obtain greater kinetic energy from the greater down-slope direction component of gravitational acceleration. This effect may cause a thicker flowing layer

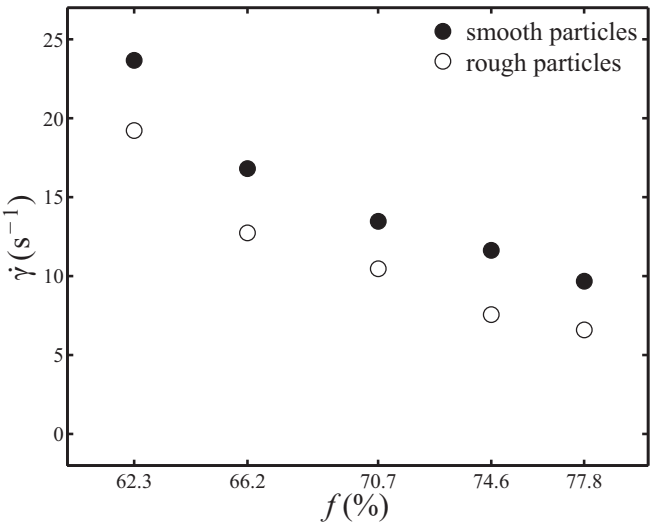

FIG. 10. The shear rate $\dot{\gamma}$ for smooth and rough particles as a function of the filling levels f.

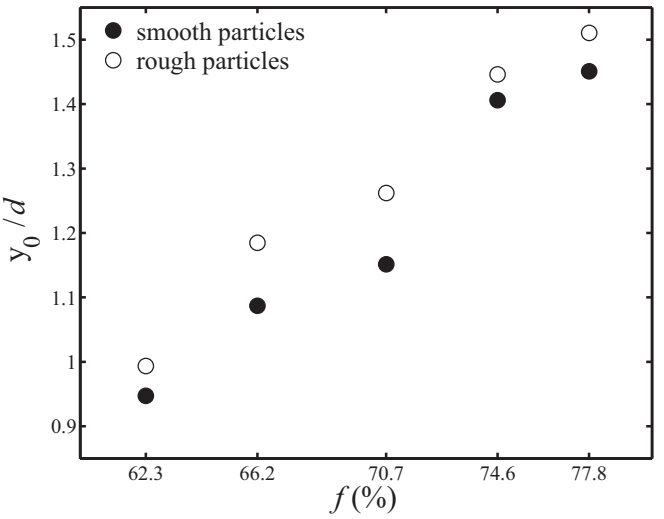

FIG. 11. The creeping region decay constant y_0 for smooth and rough particles as a function of the filling levels f.

depth. However, another opposite effect is that when the rough particles slide down the slope, the kinetic energy of the particles may be dissipated by the stronger asperities interlocking between the rough particles. Furthermore, the rough particles have lower restitution of coefficients [15], and also cause greater kinetic energy dissipation. This opposite effect may reduce the flowing layer depth. However, the result of the competition between these two contrary effects, i.e., greater driving force of gravitational acceleration and greater kinetic energy dissipation for rough particles, result in a the similar flowing layer depth for smooth and rough particles at the same filling level.

Figure 10 shows the shear rate $\dot{\gamma}$ in the flowing layer for the smooth and rough particles for five filling levels. The results were calculated from the slope of the linear part of the velocity profiles. The shear rate decreased with the fill level, which is similar to the results of Arndt *et al.* [11]. The reason for this is quite simple. For a low filling level, the half length of the free surface of the granular bed L is long (see the representation of L in Fig. 3). The longer L with a low f may cause the particle flow to easily develop from a low shear rate flow to a high shear rate flow [3]. Now, consider the surface roughness effect on the shear rate in the flowing layer. It can be seen that the shear rate was larger for smooth particles with the same filling level. The shear rate in the flowing layer can be defined as $(u_m - u_t)/\delta$, where u_m is the maximum velocity, which is at the free surface, and u_t is the velocity at the boundary between the flowing layer region and the creeping motion region. As mentioned above, when the particles slide down, kinetic energy dissipation occurs due to the collision of particles. This phenomenon may be more obvious at a position with more deep depth in the flowing layer. This is because the interparticle contact forces are stronger at a deeper position due to the extra pressure from the weight of the upper layer of particles. For this reason, at a deeper position in the flowing layer, the stronger interparticle contact forces leads to greater kinetic energy dissipation and causes the difference between the value of u_m and u_t, i.e., u_m is always larger than u_t. This difference between the value of u_m and u_t is more obvious for smooth particles, because smooth particles at the free surface have less kinetic energy dissipation and cause a larger u_m than for rough particles, while u_t for the smooth and rough particles exhibit similar values. Therefore, for a similar maximum flowing layer thickness from the results of Fig. 9, a larger difference between the value of u_m and u_t leads to a larger shear rate for smooth particles.

Finally, we will consider the dependence of the creeping region decay constant y_0 on the surface roughness of the particles. y_0 can be obtained from the fitting equation of the exponentially decaying velocity profile u_e in the creeping motion region. For a physical explanation, y_0 can represent the range of the creeping motion region [11]. Figure 11 shows y_0 for smooth and rough particles for five filling levels, where y_0 is nondimensionalized by the particle diameter. The results show that y_0 increases with filling level. This is not surprising given that the large f of a granular bed has a larger range of the creeping motion region. The reason is similar to the relation between δ and f. It is because at a large f, there are more particles that can obtain a greater rotational inertia due to the rotating driving force of the drum with a longer radius of gyration under the same rotating frequency (1 rpm). The particles with greater rotational inertia can possess greater rotational kinetic energy. With greater rotational kinetic energy of particles due to the particle revolution, there are more particles that can be dragged and slowly shifted by neighboring particles. For this reason, it may result in a longer range of the creeping region for a large f, i.e., a large value of y_0. However, this study is focused on the particle surface roughness effect. From Fig. 11, it can be seen that the rough particles have a larger y_0 and the smooth particles have a small y_0. As mentioned above, the particles are dragged and slowly shifted by neighboring particles in the creeping motion region. For the rough particles, the asperities interlocking between particles is stronger, leading to a larger drag force between particles, resulting in a longer distance of the creeping motion region and producing a larger value of y_0.

After investigating $\dot{\gamma}$, δ, and y_0, we will now we return to check the model for core precession m in Eq. (3). The dependence of m is related to a large extent on the dependence of $\dot{\gamma}$ and to a much lesser extent on y_0 and δ. However, the above discussion regarding results in Figs. 9–11 for the particles' surface roughness can explain why the rough particles exhibited a smaller core precession than the smooth particles. In other words, the reason is that the rough particles have a similar maximum flowing layer depth δ, a smaller shear rate $\dot{\gamma}$, and a larger y_0 compared to the smooth particles.

Core erosion is another important phenomenon to investigate regarding the creeping granular motion in a rotating drum with more than a half-full filling level. The model of the core dynamics, which was derived by Socie *et al.* [9], also discusses the core erosion. They derived the core erosion model based on the local diffusion coefficient. In this model, the core radius decreasing evolution, which was nondimensionalized by the particle diameter, can be described as [9]

$$\frac{r_c - r_0}{d} = -\frac{y_0}{d}\ln(N), \quad N \geqslant 5, \tag{4}$$

where r_c is the core radius and r_0 is the initial core radius after the first five revolutions. Here, $N \geqslant 5$ means that the core forms after the first five revolutions. From Eq. (4), it can be seen that the change in the core size is a logarithmic function of N with a slope of $-y_0/d$. According to Eq. (4), the error in calculating the core-erosion behavior may be of the same order as the variation in calculating the average diameter of the core circle, i.e., $\pm 4\%$. Figure 12 shows the results of the normalized change in the core size as $\ln N$. The slopes of the two dashed lines are -0.95 and -1.51 and correspond to the creeping region decay constant $y_0 = 0.95d$ from the case of $f = 0.623$ for the smooth particles and $y_0 = 1.51d$ from the case of $f = 0.778$ for the rough particles. They also represent the smallest and largest value of y_0 for all experimental cases in this paper. Thus, it is not surprising that all the data are at the locations between the two dashed lines in Fig. 12. However, the data do not follow the slope $-y_0/d$. The reason is that y_0 is obtained from the velocity profiles while Eq. (4) is based on a local diffusion coefficient, and they are quite different [9,11]. However, the values of y_0 in this paper are in a reasonable order, i.e., a few particle diameters. The tendency of the value of y_0 with the particle surface roughness and filling levels can still represent the extent of core erosion. First, Fig. 12 shows that core erosion was stronger at a larger filling level. The results also show that the core erosion was stronger when the particle surface was rough. The two dependencies of core erosion on f and particle surface roughness are both consistent with the dependence of y_0 on f and the particle surface roughness.

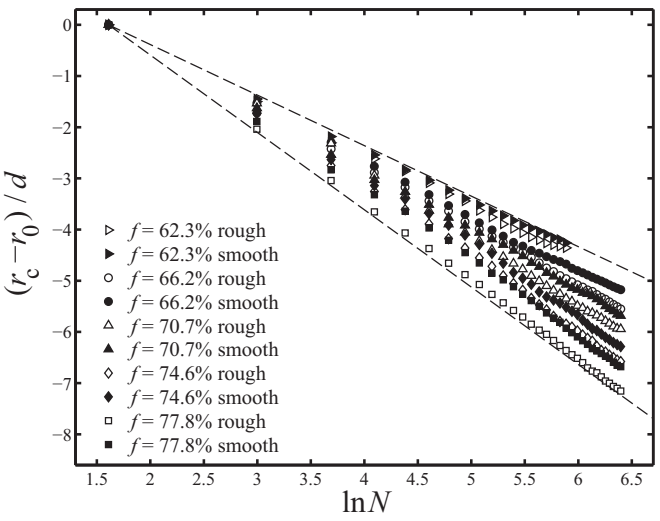

FIG. 12. The normalized change in the core size as a logarithmic function of N. The slopes of the two dashed lines are -0.95 and -1.51 and correspond to the creeping region decay constant $y_0 = 0.95d$ from the case of $f = 0.623$ for the smooth particles and $y_0 = 1.51d$ from the case of $f = 0.778$ for the rough particles.

This section further compares experimental observations with the results of model predictions with the core precessions. These results are shown in Fig. 13. Model predictions are calculated using Eq. (3), and experimental results are determined from experimental images, as shown in Fig. 4. There are large discrepancies between the core precession rates determined by the experiments and those predicted by the model, especially for small filling levels. These large discrepancies are due to the effects of particle size on the precession phenomenon. The model of core dynamics is only appropriate for illustrating the core precession behavior of smaller particles. Flowing layers drag the core and cause core rotation. The ability of smaller working particles to drag the core by the flowing layers may be low because of their denser particle arrangement structures in the core region. In other words, given the same filling level and rotation frequency, large particles have stronger core precession rates compared with small particles. To prove this argument, the same experimental process for investigating the core dynamics in this paper are conducted using smaller than

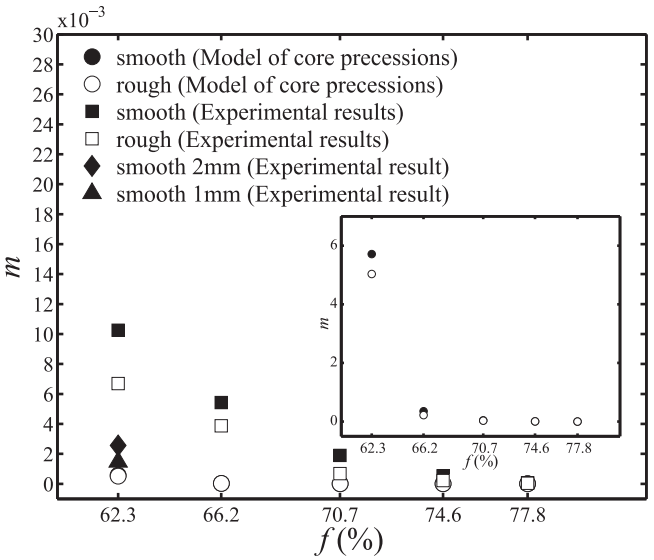

FIG. 13. Experimental observations and core dynamic model predictions of precession rate m. There are large discrepancies in the core precession rates between experimental results and model predictions, especially for small filling levels. The inset shows only results of model predictions for precession rate m. The additional results based on the experiments performed using small size particles, 1 and 2 mm, are also shown in the figure.

4 mm and smooth particles (diameters of 2 and 1 mm) at a filling level $f = 0.623$. Here we do not test small rough particles, because such particles are difficult to produce via milling. The resultant precession rate m of smooth working particles of 2 mm diameter is approximately 1/4 that of such particles of 4 mm diameter. Moreover, m of smooth working particles of 1 mm diameter is approximately 1/7 that of such particles of 4 mm diameter, as shown in Fig. 13. The results show that the precession rates for the small particles are smaller than the precession rate for the large particles, and may approach the results from the prediction model under the experimental setting of this paper. To quantify the discrepancies arising due to the effect of particle size, testing a series of particles of various sizes is necessary. However, investigation of the effects of particle size on the core precession behavior is not the main goal of this paper. This is beyond the scope of the present paper and shall not be addressed further. The relative issues that are the effect of particle sizes and interstitial fluid viscosity on the dynamics of granular creeping motion are currently being investigated by our group.

The model of core dynamics is only appropriate for illustrating the core precession behavior of small particles because this model is derived on the basis of the creeping velocity that occurs near the center of the drum. Under this assumption, large working particles, may cause the model to underestimate the precession rate. This is because large working particles have significant ability to drag the core and enable faster core rotation compared with the drum, especially at positions close and beneath the flowing layer (far from the center of the drum). This underestimation may be more obvious in cases of small filling levels because core sizes are small for small filling levels, and the effects of particle size on the precession phenomenon may be more obvious for the small cores.

IV. CONCLUSIONS

An experimental study of the particle surface roughness effect on creeping granular motion in a rotating drum was reported in this paper. The core dynamics, precession, and erosion, were measured to investigate creeping granular motion. Two different surface structures of particles were used in this paper. The discrepancy of the surface structures between the smooth and rough particles were quantified by measuring the coefficients of friction and using a simple image contrast method. The particle surface roughness effect on core precession and erosion was discussed by investigating the surface roughness effect on the shear rate $\dot{\gamma}$, the maximum flowing layer depth δ, and the creeping region decay constant y_0. In addition, the influence of the filling level on the core dynamics was also discussed.

According to the core precession model [9], the shear rate in the flowing layer $\dot{\gamma}$ dominates the extent of core precession. As mentioned by Arndt *et al.* [11], the flowing layer drags the core and causes core rotation. Therefore, when the shear rate decreases, the drag force on the core caused by the flowing layer also decreases. For a rough particle surface, the discrepancy between the velocity at the free surface and the boundary between the flowing layer and creeping motion region, u_m and u_t, is small due to the larger kinetic energy dissipation. Therefore, with a similar value of δ for the rough and smooth particles, weak core precession occurs for the rough particles.

The extent of core erosion can be described using y_0 via Eq. (4), where y_0 is obtained from the fitting equation of the exponentially decaying velocity profile u_e in the creeping motion region. y_0 represents the range of the creeping motion region. However, the particles in the creeping region exhibited diffusive displacements due to the slow creeping motion as the number of revolutions increased. The diffusive displacements can cause the slight mixing of particles (mixing with different color of particles), while the mixing particles were originally in the core with the same color of particles. Finally, particles mixing with different colors cause a decrease in the core size. Therefore, the larger value of y_0 represents the larger range of the creeping motion region and also represents larger granular diffusion and indicates stronger core erosion. In this study, although the value of y_0 calculated via the velocity profile was different from the changing rate of the core size, the dependencies of y_0 on the particle surface roughness and filling levels still illustrates the dependence of core erosion on the particle surface roughness and filling levels.

A comparison of the core precessions predicted by the model [9] with the experimental observations indicates that the precession rate m depends on particle size. Under the assumption that the creeping velocity occurs near the center of the drum, the model can be simplified, as shown in Eq. (3). Given Eq. (3), the model can still be used for the qualitative analysis of the influence of different particle characteristics on core dynamics. However, the work in this paper well connects the physical relation between the particle surface roughness and creeping granular motion. Furthermore, this paper also provided some important observations regarding the particle surface roughness on the dynamics of granular flow. These physical arguments can also be applied to other future investigations on granular flow, e.g., granular chute flow, granular flow in a vibrating bed, granular flow in a silo, etc.

ACKNOWLEDGMENTS

The work was supported by the Ministry of Science and Technology, Taiwan (Republic of China), under Grant No. MOST103-2221-E-008-042-MY3. The authors wish to express their sincere thanks to Dr. S. H. Chou, Department of Mechanical Engineering, National Central University (NCU), Taiwan (Republic of China), for in-depth discussions. The authors also would like to thank Enago (www.enago.tw) for the English language review.

APPENDIX: PROCEDURE USED FOR PIV ANALYSIS

Particle image velocimetry (PIV) has been adapted to measure particle displacement and velocity field in granular flows [32–36]. In this paper, we used the PIV technique (proVISION-XS software by IDT Co.) to measure the velocity field of granular mediums in the rotating drum. This technique is based on an optical measuring system and its experimental setup typically comprises several subsystems. The first is a moving granular system with sufficient illumination. In this paper, the inner diameter of the circular container locking

on the rotating drum is 50 cm and the total granular medium in this container is illuminated by four LED lamps (100 W, 6000 K) in order to produce uniform and adequately illuminated images that are captured with the high-speed camera. More importantly, under this illumination condition, the experimental images also have a sufficiently sharp image contrast to increase the accuracy of the PIV analysis [35]. The second subsystem is a monoscopic (single-lens) high-speed CMOS camera (IDT MotionPro Y3 plus, monochrome, with a shooting frame rate of 2000 fps and a resolution of 1280×1024 pixels), which is used to capture the sequential digital images of the moving granular system. The third subsystem is the computer connected to the camera, which is used for data storage and PIV analysis.

The typical approach involved in acquiring images using a high-speed camera for PIV analysis is to record two images in one frame. This is known as *single-frame double-exposure recording* [37]. The time interval between the two images, Δt, is very short and is usually of the order of 1 ms. Displacement of identifiable particles or group of pixels between the two images are calculated using a very complicated probabilistic algorithm that is based on a cross-correlation scheme. The displacement divided by Δt is the velocity of this identifiable particles or group of pixels. However, a suitably modified PIV technique has the capability to combine two successive digital frames with individual exposure into a single frame. This is known as *two-frame, single-exposure recording* . In this paper, we adopted the latter recording process to calculate the particle velocities. First, the high-speed camera captures the sequential experimental frames at a frame rate of 2000 fps. The PIV system then combines every two successive frames into a single new frame. The particle velocity fields are calculated using each new combined frame. Finally, the time-averaged velocity fields, see Fig. 7, are obtained by averaging all velocity fields that are calculated using each newly combined frame.

Under our camera exposure settings, the displacements of the particles between two successive images are approximately a particle size in radius, which corresponds to approximately six pixels in the image. This enables us to set the optimal size of the interrogation window of the PIV scheme to approximately four times the particle displacement in successive images [38]. Therefore, in the current study, the interrogation window is set at of 24 pixels $\times$ 24 pixels. This yields a fine resolution for the velocity field.

Conversely, PTV is another popular method used to calculate the velocity of granular flow. It offers the advantage of tracking the individual particles and then calculating their velocities. However, the limitation of PTV is the low image resolution. In order to track the individual particles using the PTV method, every individual particle in the experimental image should be clear and discernible. For the resolution of the experimental images in this paper, it is difficult to calculate the granular velocity using PTV. Conversely, our experimental images have sufficiently sharp image contrast and can provide a good accuracy for the PIV analysis. Therefore we only focused on the PIV scheme in this paper.

[1] H. M. Jaeger, S. R. Nagel, and R. P. Behringer, Rev. Mod. Phys. **68**, 1259 (1996).
[2] A. Aradian, E. Raphaël, and P. G. de Gennes, Phys. Rev. E **60**, 2009 (1999).
[3] A. V. Orpe and D. V. Khakhar, Phys. Rev. E **64**, 031302 (2001).
[4] J. Mellmann, E. Specht, and X. Liu, AICHE J. **50**, 2783 (2004).
[5] T. S. Komatsu, S. Inagaki, N. Nakagawa, and S. Nasuno, Phys. Rev. Lett. **86**, 1757 (2001).
[6] N. Jain, J. M. Ottino, and R. M. Lueptow, Phys. Fluids **14**, 572 (2002).
[7] K. M. Hill, G. Gioia, and V. V. Tota, Phys. Rev. Lett. **91**, 064302 (2003).
[8] A. V. Orpe and D. V. Khakhar, Phys. Rev. Lett. **93**, 068001 (2004).
[9] B. A. Socie, P. Umbanhowar, R. M. Lueptow, N. Jain, and J. M. Ottino, Phys. Rev. E **71**, 031304 (2005).
[10] J. J. McCarthy, T. Shinbrot, G. Metcalfe, J. E. Wolf, and J. M. Ottino, AIChE J. **42**, 3351 (1996).
[11] T. Arndt, A. Brucks, J. M. Ottino, and R. M. Lueptow, Phys. Rev. E **74**, 031307 (2006).
[12] G. Metcalfe, T. Shinbrot, J. J. McCarthy, and J. M. Ottino, Nature (London) **374**, 39 (1995).
[13] N. A. Pohlman, B. L. Severson, J. M. Ottino, and R. M. Lueptow, Phys. Rev. E **73**, 031304 (2006).
[14] G. Plantard, H. Saadaoui, P. Snabre, and B. Pouligny, Europhys. Lett. **75**, 335 (2006).
[15] C. C. Liao, S. S. Hsiau, and C. S. Wu, Phys. Rev. E **86**, 061316 (2012).
[16] Y. L. Ding, R. N. Forster, J. P. K. Seville, and D. J. Parker, Chem. Eng. Sci. **56**, 3737 (2001).
[17] A. Bodrova and N. Brilliantov, Granul. Matter **14**, 85 (2012).
[18] M. P. Ciamarra, M. D. De Vizia, A. Fierro, M. Tarzia, A. Coniglio, and M. Nicodemi, Phys. Rev. Lett. **96**, 058001 (2006).
[19] S. Ulrich, M. Schröter, and H. L. Swinney, Phys. Rev. E **76**, 042301 (2007).
[20] N. Jain, J. M. Ottino, and R. M. Lueptow, Granul. Matter **7**, 69 (2005).
[21] A. A. Boateng and P. V. Barr, J. Fluid Mech. **330**, 233 (1997).
[22] J. R. Ferron and D. K. Singh, AICHE J. **37**, 747 (1991).
[23] S. H. Chou, C. C. Liao, and S. S. Hsiau, Phys. Fluids **23**, 083301 (2011).
[24] H. Henein, J. K. Brimacombe, and A. P. Watkinson, Metall. Trans. **14**, 191 (1983).
[25] J. Rajchenbach, Phys. Rev. Lett. **65**, 2221 (1990).
[26] J. M. Ottino and D. V. Khakhar, Annu. Rev. Fluid Mech. **32**, 55 (2000).
[27] J. Mellmann, Powder Technol. **118**, 251 (2001).
[28] S. H. Chou and S. S. Hsiau, Powder Technol. **226**, 99 (2012).
[29] N. Jain, J. M. Ottino, and R. M. Lueptow, J. Fluid Mech. **508**, 23 (2004).
[30] D. Bonamy, F. Daviaud, and L. Laurent, Phys. Fluids **14**, 1666 (2002).

[31] S. Courrech du Pont, R. Fischer, P. Gondret, B. Perrin, and M. Rabaud, Phys. Rev. Lett. **94**, 048003 (2005).
[32] D. M. Hanes and O. R. Walton, Powder Technol. **109**, 133 (2000).
[33] S. P. Pudasaini, S. S. Hsiau, Y. Wang, and K. Hutter, Phys. Fluids **17**, 093301 (2005).
[34] S. P. Pudasaini, K. Hutter, S. S. Hsiau, S. C. Tai, Y. Wang, and R. Katzenbach, Phys. Fluids **19**, 053302 (2007).
[35] L. T. Sheng, C. Y. Kuo, Y. C. Tai, and S. S. Hsiau, Exp. Fluids **51**, 1329 (2011).
[36] C. Y. Kuo, L. T. Sheng, S. Y. Chiu, Y. Z. Yang, Y. C. Tai, and S. S. Hsiau, Phys. Fluids **27**, 013305 (2015).
[37] R. J. Adrian and J. Westerweel, *Particle Image Velocimetry* (Cambridge University Press, Cambridge, England, 2011).
[38] R. J. Adrian, Appl. Opt. **25**, 3855 (1986).